# The lightning swept stroke along an aircraft in flight. Part I: thermodynamic and electric properties of lightning arc channels

Larsson, A; Lalande, P; Bondiou-Clergerie, A; Lalande, P; Delannoy, A

*Published in:*
Journal of Physics D: Applied Physics

*DOI:*
10.1088/0022-3727/33/15/317

2000

The lightning swept stroke along an aircraft in flight. Part I: thermodynamic and electric properties of lightning arc channels



2000 J. Phys. D: Appl. Phys. 33 1866

(http://iopscience.iop.org/0022-3727/33/15/317)

J. Phys. D: Appl. Phys. **33** (2000) 1866–1875. Printed in the UK PII: S0022-3727(00)11287-2

# The lightning swept stroke along an aircraft in flight. Part I: thermodynamic and electric properties of lightning arc channels

**Anders Larsson†, Philippe Lalande, Anne Bondiou-Clergerie‡ and Alain Delannoy**

Office National d'Etudes et de Recherches Aérospatiales,
BP 72–29 Avenue de la Division Leclerc, F-92322 Châtillon CEDEX, France

E-mail: bondiou@onera.fr

Received 24 January 2000

**Abstract.** During a lightning strike to an aircraft in flight, the lightning channel becomes deformed in the airflow and displaced along the aircraft, a so-called *swept stroke*. The deformation and the displacement are caused by the interaction between the aerodynamic flow and the plasma properties of the channel together with the properties of the surface. The main part of the lightning current is a continuous current with a magnitude of hundreds of amperes and a duration of hundreds of milliseconds. The objective of this article is to analyse the properties of the lightning channel during this continuous current phase in order to parametrize them; this parametrization is used in a companion paper (Larsson *et al J. Phys. D: Appl. Phys.* **33** 1876–83) for complete swept-stroke simulations. A model of the thermodynamic evolution of a lightning channel during its continuous current phase is developed and numerically solved. In this model, the channel is assumed to have axial symmetry. A quantitative analysis of the influence of failing axial symmetry is also included. The main conclusions are that the steady-state conditions are rapidly reached and that the channel can be considered to be a free-burning arc subjected to increased thermal losses due to transverse aerodynamic flow.

## 1. Introduction and phenomenology of the problem

A lightning strike is a natural electrical discharge and lightning strikes to aircraft are frequent and unavoidable events. On average, every civilian airliner is struck by lightning about once per year. Thus, the issue of lightning protection of aircraft is of utmost importance. To understand the threat, instrumented aircraft have been flown into thunderstorms to measure the lightning strike event (Bailey and Anderson 1987, Boulay 1994), and the results have been collected into a public database (Uhlig *et al* 1999). These in-flight data were been analysed by Lalande *et al* (1999a).

The in-flight measurements have shown that there are two types of lightning strike to aircraft. The most frequent type observed (90% of all events) is when the aircraft itself triggers a lightning discharge. When the aircraft enters a region of high ambient electric field, the field enhancement at the extremities of the aircraft initiates corona discharges and eventually a positive leader is initiated. During its propagation, the aircraft becomes negatively charged and eventually a negative leader is incepted at an opposing extremity. This bi-directional leader constitutes the beginning of a lightning flash. The second type is when the aircraft intercepts a natural lightning channel.

During a lightning flash, the aircraft forms a part of the discharge path. Therefore, there are two attachment points on the aircraft, one entry point and one exit point, for the lightning current. A typical current of the lightning strike has been extracted from the in-flight measurement database (figure 1). The figure shows an average of several in-flight measurements. It consists of an initial positive leader current of about 1 A (phase ① in figure 1) followed by superimposed current impulses (②). After the initiation of the negative leader, the bi-directional leader conducts a continuous current of about 300 A which lasts for around 200 ms (③). High-amplitude current impulses are superimposed on this continuous current (④). Eventually, the continuous current stops and only the high-amplitude current impulses occur (⑤) separated by zero-current intervals (⑥). The in-flight current measurements show large similarities with current measurements of triggered lightning using a

† Present affiliation: Division of Atomic Physics and Division of Combustion Physics, Lund Institute of Technology, PO Box 118, S-221 00 Lund, Sweden.
‡ Author to whom correspondence should be addressed.

0022-3727/00/151866+10$30.00 

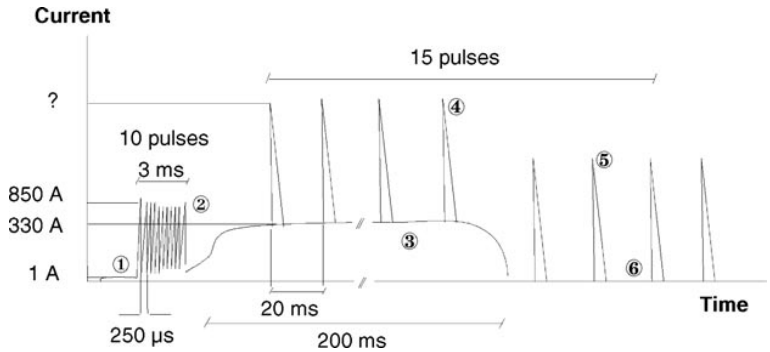


**Figure 1.** Typical waveform of the discharge current during a lightning strike to an aircraft where the aircraft itself initiates the lightning discharge. The waveform is the average of several current oscillograms obtained during the in-flight measurements. The different phases are numbered and are described in the text. From Lalande *et al* (1999a).

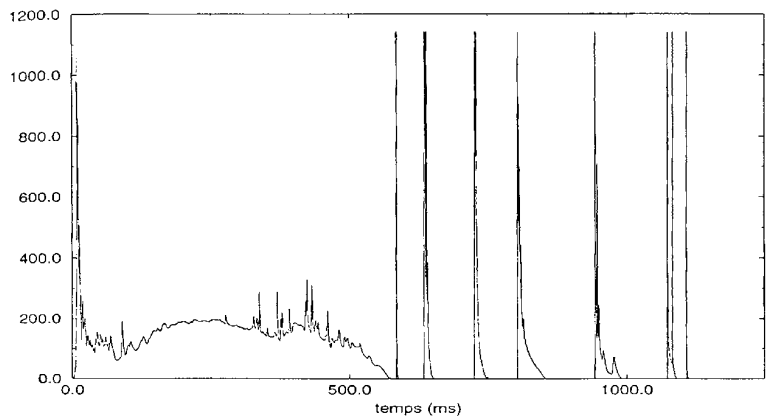


**Figure 2.** A measured current waveform of rocket-triggered lightning showing large similarities with the in-flight measurements (cf figure 1). From Lalande (1996).

rocket and earthed wire system, as shown in figure 2 (Lalande *et al* 1998).

The lightning channel is essentially stationary in the air while the aircraft is moving. Since the duration of the lightning flash is of the order of 100 ms, the lightning channel can be displaced along the whole aircraft length (aircraft length and speed are of the order of 10 m and 100 $ms^{-1}$, respectively). If one of the attachment points is located at, for instance, the radome, the lightning channel will sweep back along the aircraft fuselage. This is known as a *swept stroke*. Figure 3 is an extract from a video film, taken during one of the in-flight campaigns, showing a lightning strike to an aircraft in flight where the lightning channel sweeps underneath the aircraft. The properties of the surface influence how the channel sweeps along it and determine the different attachment points and the time the channel dwells at these points. The currents fed into the aircraft at these attachment points are potential safety hazards for the aircraft. Thus, the determination of how the attachment point may sweep along the aircraft surface and the division of the aircraft surface into zones of different lightning current threats constitutes a vital task for the designer of lightning protection systems. The discharge initiation and initial attachment of the lightning channel to the aircraft are rapid processes and have been successfully simulated by neglecting any sweeping phenomena (Lalande *et al* 1999b, c). Zaglauer *et al* (1999) discuss the phenomenology of the lightning swept stroke and how it might be numerically simulated. However, no simulations of the swept stroke were presented by Zaglauer *et al* and no simulations have been found elsewhere in the literature. This lack of work done in this field might be due to its complex and multi-disciplinary character. When the aircraft moves, two phenomena may occur at the attachment point, depending on the surface properties, the aerodynamic flow profile close to the surface and the plasma properties of the channel. First, the attachment point may dwell at the same spot and thus follow the aircraft as it moves through the air (figure 4(a)). This results in a large deformation of the lightning channel. Second, the attachment point may continuously sweep along the surface (figure 4(b)). Another important phenomenon is the possibility of having a reattachment (or re-connection) between a segment of the channel and the surface (figure 4(c)). The voltage distribution along the channel is dependent on the lightning current and the plasma properties of the channel. This voltage distribution gives rise to the possibility of an electric breakdown between the surface and a part of the channel some distance away from the surface. At such a breakdown, the channel attachment point makes a jump. Reattachment can occur if the channel is substantially deformed or if the channel sweeps along a complex object where reattachment may occur on protruding parts.

The work is presented in two parts. In this paper (part I), the properties of the lightning channel during the continuous

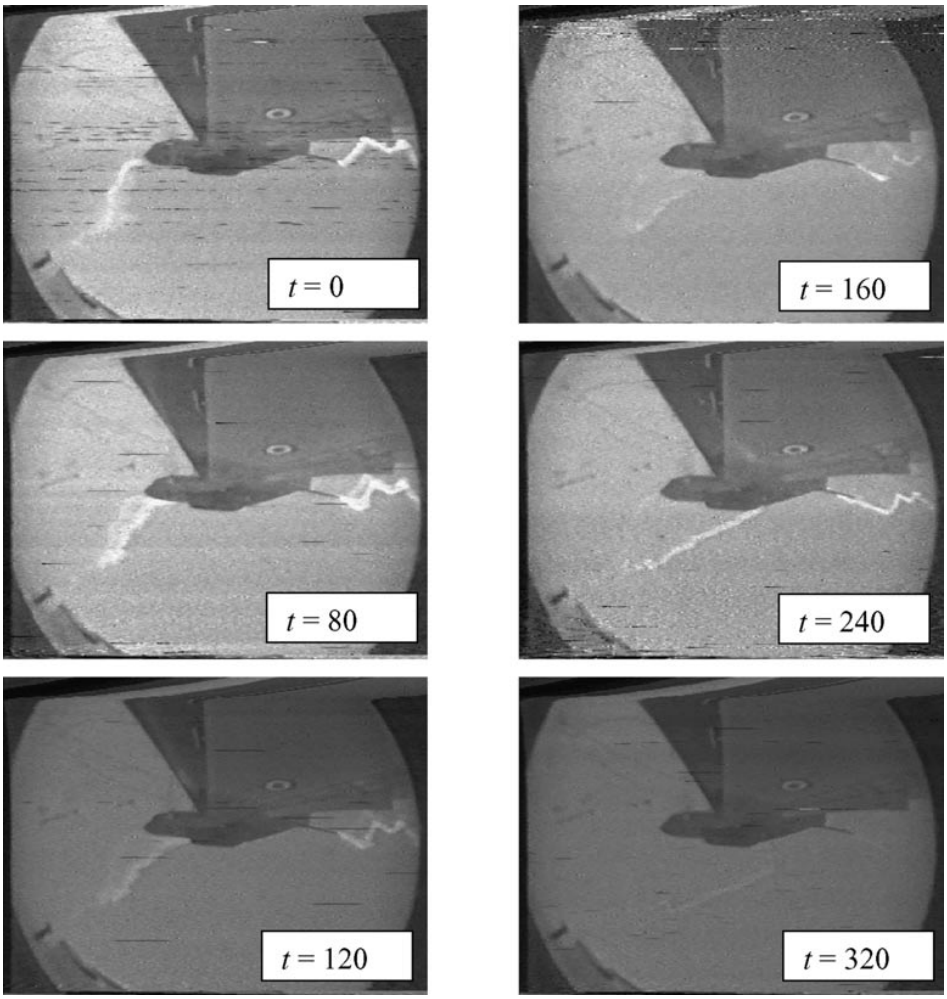


**Figure 3.** Extract from a video film showing how a lightning channel sweeps along a Transall aircraft in flight when struck by lightning. The video camera had a wide-angle lens and was mounted under the wing, close to its tip. At $t = 0$, the lightning channel has two attachment points, one at the front and one at the rear. Thus, the aircraft forms a part of the discharge path. At $t > 0$, the forward attachment point sweeps backwards along the fuselage due to the movement of the aircraft.

current phase are analysed. The second part (Larsson *et al* 2000) describes the different features of the numerical modelling of the sweeping process and compares the output of the calculations with existing experimental data. The work presented here is a part of the continuing efforts performed by ONERA and its partners to increase the understanding of the lightning discharge and how to numerically model it. These efforts have resulted in studies of the positive discharges by Bondiou and Gallimberti (1994), Goelian *et al* (1997) and Larsson *et al* (1998), negative discharges by Bacchiega *et al* (1994) and bi-directional discharges by Castellani *et al* (1998a, b).

The lightning channel is sufficiently long so that its characteristics are governed by processes in the arc plasma column rather than by electrode processes. In this paper, the modelling of the sweeping process will be performed considering only the continuous current phase (phases ① and ③ in figure 1). The theoretical analysis is based on studies of the steady-state conditions of an arc column (Bublievski 1978, Jones 1983, Raizer 1997). Modelling of the swept stroke during current impulses and during zero-current intervals will be the subject of future research. This paper presents a model of the thermodynamic evolution of a lightning channel during its continuous current phase where the channel is assumed to have axial symmetry (section 2) and an analysis of the influence of failing axial symmetry (section 3). SI units are used in all equations throughout this paper. When the original references give formulae in non-standard units, the formulae have been converted into SI units.

## 2. Arc channel with axial symmetry

### 2.1. Arc column model

The model outlined below is based on the laws of hydrodynamical conservation, which are supposed to be valid if the departures from local thermodynamic equilibrium (LTE) are small (Vérité *et al* 1995). Although such an assumption is not always justified for the arc discharge, experience from numerical and physical experiments indicates that such a model can correctly predict the behaviour of the core of the arc (Uman and Voshall 1968, Lowke *et al* 1973, Delalondre and Simonin 1990, Raizer

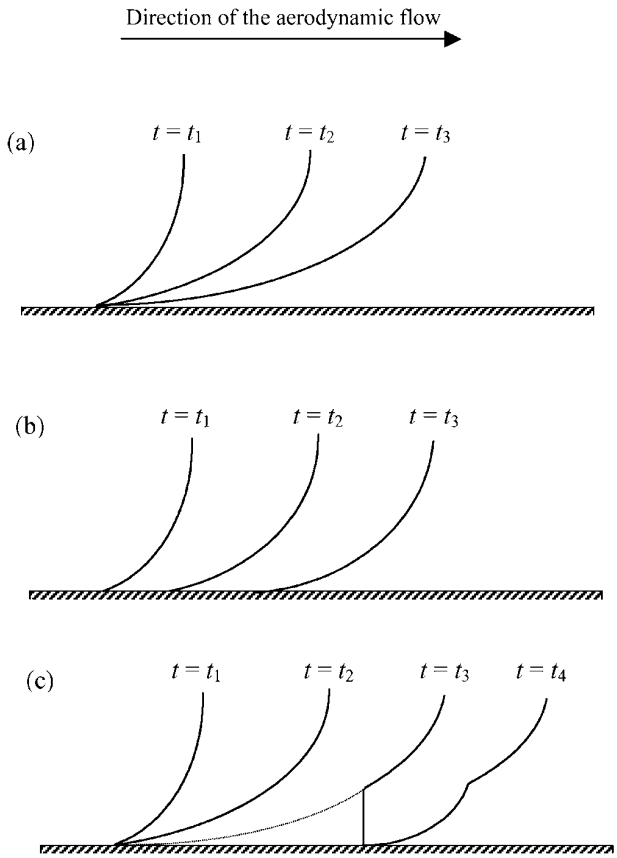


**Figure 4.** Illustrations of three different swept-stroke phenomena. The lines represent the position of the lightning channel. (a) The attachment point dwells at the same spot, (b) the attachment point sweeps continuously along the surface and (c) a breakdown occurs between the channel and the surface (at $t = t_3$) and the attachment point makes a jump (a reattachment). The broken curve shows the short-circuited part of the channel.

1997). Furthermore, high-amplitude currents precede the continuous current in the lightning channel. This means that the central core of the lightning channel has been intensively heated and the LTE is maintained (Gallimberti and Stangherlin 1986). The deviation from LTE in free-burning arcs as discussed by Haidar (1999) was caused by local effects close to the cathode. The implication of the assumption of LTE is that there is a unique temperature for every kind of particle, which makes it possible to treat the arc plasma as a one-phase medium having a well defined velocity, pressure and temperature (or enthalpy) at each point. The arc plasma is thus treated as a Newtonian fluid including electromagnetic effects.

The balance equations for mass, momentum and energy can be written as (Vérité *et al* 1995)

$$\frac{\partial \rho}{\partial t} + \nabla \cdot (\rho \boldsymbol{v}) = 0 \tag{1}$$

$$\rho \frac{\partial v}{\partial t} + \rho(\boldsymbol{v} \cdot \nabla)\boldsymbol{v} = -\nabla p + \nabla \cdot \boldsymbol{T} + \boldsymbol{f}_{em} \tag{2}$$

and

$$\rho \frac{\partial h}{\partial t} + \rho \boldsymbol{v} \cdot \nabla h = \frac{\partial p}{\partial t} + \boldsymbol{v} \cdot \nabla p - \nabla \cdot Q - S_r + P_J \tag{3}$$

with the equation of state

$$\rho = F(T, p) \tag{4}$$

where $\rho$ is the mass density, $\boldsymbol{v}$ is the velocity of the gas, $p$ is the pressure, $\boldsymbol{T}$ is the momentum diffusion tensor, $\boldsymbol{f}_{em} = \boldsymbol{j} \times \boldsymbol{B}$ is the electromagnetic force density (or the Lorentz force density), $h$ is the enthalpy per unit mass, $Q$ is the thermal diffusion flux, $S_r$ are the radiative losses, $P_J = \boldsymbol{j} \cdot \boldsymbol{E} = \sigma E^2$ is the Joule source term with $E$ as the internal electric field of the arc plasma, $T$ is the temperature, $\boldsymbol{j}$ is the current density, $\boldsymbol{B}$ is the magnetic flux density and $\sigma$ is the electrical conductivity.

The Lorentz force $\boldsymbol{f}_{em}$ is only important for currents about and above 10 kA. For instance, the magnetic pressure due to the Lorentz force is less than 1% of the atmospheric one for arc currents of 500 A and a channel radius of 5 mm (Jones 1983). Thus, the Lorentz force is neglected. The thermal diffusion flux is assumed to be given by $Q = -\kappa \nabla T$, where $\kappa$ is the thermal conductivity. Here the relation between the enthalpy and the temperature can be appropriately approximated by $c_p \partial T = \partial h$, where $c_p$ is the heat capacitivity (heat capacity per unit mass) of the gas at isobaric transformations. Furthermore, the cooling of the channel occurs sufficiently slowly to assume that pressure equilibrium is realized everywhere (Gallimberti and Stangherlin 1986). This means that the pressure is constant in the channel and is equal to the ambient pressure, implying that the momentum balance equation (2) can be omitted and that the derivatives of the pressure disappear in the energy balance equation (3). (Comparison with a non-isobaric model (Berton 1995) indicates small differences in calculated quantities.) The remaining equations are the mass-balance and the energy-balance equations

$$\frac{\partial \rho}{\partial t} + \nabla \cdot (\rho \boldsymbol{v}) = 0 \tag{5}$$

$$\rho c_p \left( \frac{\partial T}{\partial t} + \boldsymbol{v} \nabla T \right) = \nabla \cdot (\kappa \nabla T) + \sigma E^2 - S_r. \tag{6}$$

The internal electric field $E$ is related to the lightning current $I$ as

$$I = 2\pi E \int_0^R \sigma r \, \mathrm{d}r. \tag{7}$$

Numerical values of the thermal and electrical conductivities are taken from Lowke *et al* (1973). The radiative losses are the sum of the retardation radiation and the recombination radiation, and can be expressed as (Braginskii 1958)

$$S_r = S_{ret} + S_{rec} = 3.48 \times 10^{-40} n_e^2 T^{0.5} + 1.35 \times 10^{-34} n_e^2 T^{-0.5} \tag{8}$$

where $n_e$ is the electron number density. The electron number density is calculated using Saha's equation in the following form (Les Renardières Group 1977):

$$n_e = 4.768 \times 10^{10} T^{0.75} n^{0.5} \exp(-90\,420/T) \tag{9}$$

where $n$ is the gas number density.

These equations are closed by the ideal gas state equation

$$p = \rho R' T \tag{10}$$

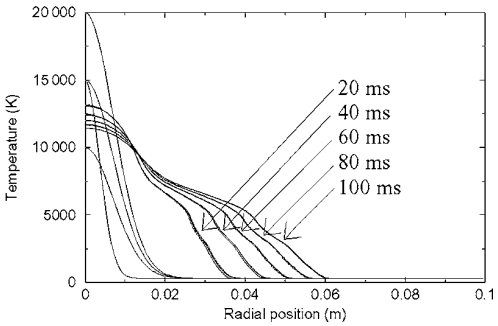


**Figure 5.** Temperature profiles for four different choices of initial profiles of the temperature ($T_{max0} = 20$ kK, $a = 10$ mm; $T_{max0} = 15$ kK, $a = 10$ mm; $T_{max0} = 10$ kK, $a = 10$ mm; $T_{max0} = 15$ kK, $a = 5$ mm) at a current $I = 500$ A. The differences in the initial profiles have minor effect on the later profiles.

where $p$ is the pressure (here considered as a constant, see above) and $R' = R/M$ with $R$ as the molar gas constant ($R = 8.32$ J K$^{-1}$ mol$^{-1}$) and $M$ as the molar mass of the gas. For cold air, $M = 0.029$ kg mol$^{-1}$. The molar mass of air as a function of temperature has been calculated, and the calculations are outlined in the appendix.

Assuming a cylindrical plasma channel, closely following Gallimberti and Stangherlin (1986), one can write the system as

$$\begin{cases} \rho c_p \dfrac{\partial T}{\partial t} = \kappa \dfrac{\partial^2 T}{\partial r^2} + \left( \dfrac{\kappa}{r} + \dfrac{\partial \kappa}{\partial r} - \rho c_p v_r \right) \dfrac{\partial T}{\partial r} + \sigma E^2 - S_r \\ \rho v_r = -\dfrac{1}{r} \dfrac{\partial}{\partial t} \left( \displaystyle\int_0^r r' \rho \, \mathrm{d}r' \right). \end{cases} \tag{11}$$

The initial and boundary conditions for the temperature and the mass velocity are required. The initial condition for the temperature was a Gaussian distribution

$$T(r, 0) = T_{amb} + (T_{max0} - T_{amb}) \exp(-r^2/a^2) \tag{12}$$

where $T_{amb}$ is the ambient temperature and $T_{max0}$ is the initial temperature of the centre of the plasma channel. The Gaussian temperature profile is consistent with the radial density profile derived from Schlieren pictures of leader channels (Gallimberti and Stangherlin 1986). The initial mass velocity was equal to the diffusion velocity:

$$\rho v_r = -D \frac{\partial \rho}{\partial r} \tag{13}$$

with $D = 10^{-4}$ m$^2$ s$^{-1}$. However, the results are not sensitive to the chosen initial condition of the mass velocity. The boundary conditions at the channel axis are given by

$$\begin{cases} \left. \dfrac{\partial T}{\partial r} \right|_{r=0} = 0 \\ v_r(0, t) = 0 \end{cases} \tag{14}$$

A straightforward explicit Euler time-stepping algorithm is used to solve this system (Berton 1995).

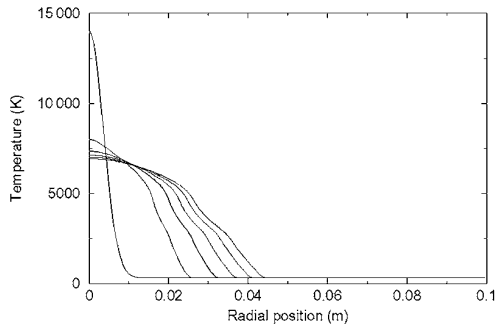


**Figure 6.** The profiles of the temperature at different instants of time for an arc current of 100 A and $t = 0$, 20, 40, 60, 80 and 100 ms.

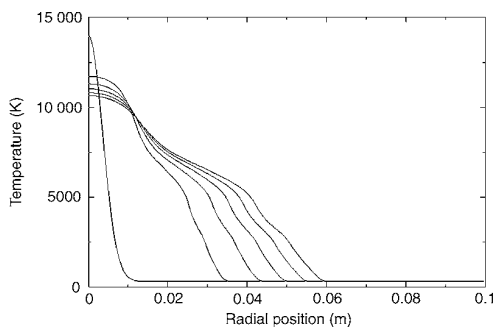


**Figure 7.** Temperature profiles under the same conditions as figure 6, but with a current of 500 A.

### 2.2. Results

The sensitivity of the results for changes in the initial temperature profile was checked by varying the initial temperature maximum $T_{max0}$ and the Gaussian radius $a$. The temperature and radius of a lightning return stroke are about 30 kK and less than 10 mm, respectively (Uman and Voshall 1968). Corresponding values for the laboratory leader channel are 5 kK and 1 mm (Gallimberti 1979). The initial properties of the lightning channel before the continuous current phase lies probably somewhere in between these values. Figure 5 shows four simulations in the case of a constant current of 500 A with four different initial conditions ($T_{max0} = 20$ kK, $a = 10$ mm; $T_{max0} = 15$ kK, $a = 10$ mm; $T_{max0} = 10$ kK, $a = 10$ mm; $T_{max0} = 15$ kK, $a = 5$ mm) at six different times ($t = 0$, 20, 40, 60, 80 and 100 ms). The figure reveals that at 20 ms and onward, the temperature profiles overlap. Thus, the choice of the initial temperature profile has no significant effect on the later profiles.

Simulations for an initial temperature maximum of 14 kK and a channel temperature profile with a Gaussian radius of 5 mm are presented in figures 6–8. Figure 6 shows the temperature profile of the channel at different times for a lightning current of 100 A. Figure 7 shows the same, but for a current of 500 A. The development in time of the internal electric field, given by equation (7) for both currents, are presented in figure 8. The temperature profile plots show that the channel quickly expands to a radius of several tens of millimetres and is in the range of 20–60 mm for the current and the time scales of interest. The internal electric field quite quickly approaches a relatively stable value. Experimental data for the internal field in long

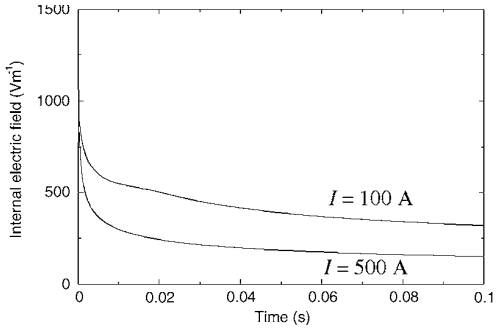


**Figure 8.** The development over time of the internal electric field for two different arc currents.

(50–500 mm) steady-state free-burning arcs are given by von Engel (1955). In the current range of 0.1–1 kA, the internal electric field of an arc channel is 200–150 V m$^{-1}$, thus being only slightly dependent on the magnitude of the current. The simulation gives a larger dependency, but the magnitude of the internal electric field is in good agreement with the measurements. Thus, for these steady-state arcs, the assumption of a cylindrical plasma channel is validated.

However, Dobbing and Hanson (1978) present experimental estimations of the internal electric field in the arc channel using data extracted from two different swept-stroke experiments. In the first experiment, they forced the movement of the arc channel over a stationary surface sample by means of an imposed magnetic field that gave rise to a Lorentz force acting on the channel. The internal electric field was measured to be $E_{arc} = 2.4 \pm 0.48$ kV m$^{-1}$ for a triangularly-shaped current with an amplitude of 3 kA with a duration of 30 ms. In the second experiment, they displaced a surface sample relative to the arc channel, where the channel was at rest in the air frame of reference. The surface was a wing dummy mounted on a rocket sled running on a railway track. An internal electric field of $E_{arc} = 1.34 \pm 0.44$ kV m$^{-1}$ was determined for continuous currents in the range 300–600 A. The magnitude of the internal electric field from this experiment differs significantly from the steady-state internal electric field presented above. The possible reasons for this discrepancy are analysed in the following section.

## 3. Arc channel in transverse aerodynamic flow

One important circumstance that is not included in the arc column model presented in the previous section is that the lightning channel is, at least partly, subjected to a transverse aerodynamic flow. This flow displaces and deforms the channel. Now, one must be very precise by what one means by the position of an arc channel. The motion of the arc channel can be described as a temperature cloud where the motion is divided into two parts, one being the relative velocity of the arc phenomenon with respect to the mass flow and the other the mass motion itself (Maecker 1971). With this distinction, an appropriate definition of the position of the channel is the position of its temperature maximum. The motion of the arc channel is then identical to the displacement of this position. In this way the arc channel is in fact viewed as a 'heat wave'. The velocity of the position of the temperature maximum of the arc channel $v_a$ can thus be divided into two components

$$v_a = v_{am} + v_m \tag{15}$$

where $v_{am}$ is the relative velocity of the position of the maximum temperature with respect to matter and $v_m$ the mass velocity. $v_{am}$ is determined by the internal energy equation and is zero for situations with axial symmetry of the channel. Furthermore, in a transverse aerodynamic flow, the channel can be assumed to have an impermeable core so that the channel can be treated as a solid cylindrical body (Bublievskii 1978). Three effects that are not included in the arc column model given in the previous section will be analysed in this section: the bending of the arc channel, the elongation of it and, finally, the increased thermal losses introduced by the aerodynamic flow.

### 3.1. Anti-bending of a curved arc

The most important cause of failing axial symmetry in the energy balance equation is the bending of the arc channel (figure 9). The bending of the channel concentrates the current density and heat conduction to the inner side, thus giving rise to a displacement of the temperature maximum towards the inner side of the channel. The net effect is a tendency to straighten out the bent arc. A simple formula for the velocity of this 'anti-bending' was derived by Maecker (1971)

$$v_{am} = -5k\frac{\kappa}{nC_p} \tag{16}$$

where $k$ is the curvature of the channel (that is, the inverse of the curvature radius), $n$ is the heavy-particle number density and $C_p$ is the heat capacity at isobaric transformations. Figure 10 shows the anti-bending velocity as a function of the curvature at two different channel temperatures ($T = 5$ and 10 kK, respectively). Equation (16) gives the fact that the curvature must be larger than 100 m$^{-1}$ to give rise to a significant anti-bending velocity when comparing it to typical aircraft velocities, which are of the order of 100 ms$^{-1}$. A curvature of 100 m$^{-1}$ is equivalent to a curvature radius of 10 mm. Hence, for the anti-bending to be of importance, there must be a very sharp turn in the arc channel. Consequently, the error introduced by neglecting the anti-bending is small. On the other hand, it is straightforward to include (16) in any swept-stroke simulation.

### 3.2. Elongation of the channel

During the swept stroke, the arc channel might be elongated: the length, and thereby the volume, of the channel increases. This elongation cannot be directly included into the arc column model presented in section 2.1 since the elongation is a process in the axial direction. However, the channel elongation can be introduced as an artificial energy loss term, $Q_{elo}$, in the energy-balance equation (3). $Q_{elo}$ is estimated in the following way. First, assume that the pressure remains constant within the elongated channel. Furthermore, when the channel is elongated, let the volume increase of the channel be d$V$. If assuming that this extra volume of air

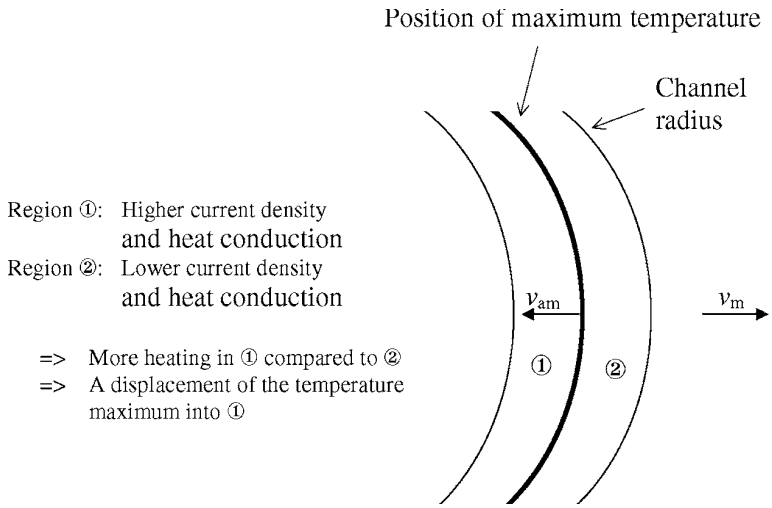


**Figure 9.** Physical explanation of why a curved arc channel is straightened out. $v_{am}$ is the anti-bending velocity and $v_m$ is the mass velocity.

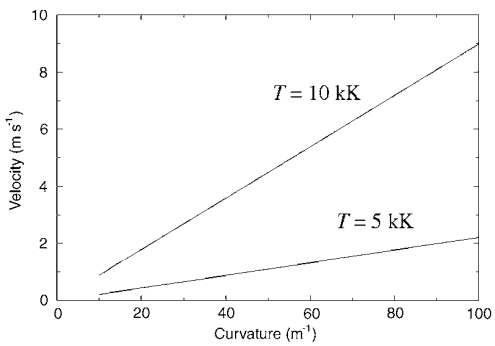


**Figure 10.** The anti-bending velocity as a function of the channel curvature for two different temperatures.

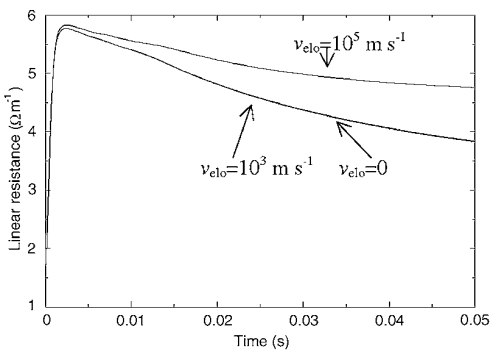


**Figure 11.** The development over time of the linear resistance of the arc channel at different magnitudes of the elongation velocity $v_{elo}$ for a current of 100 A. Note that the curves for $v_{elo} = 0$ and 1 km s$^{-1}$ overlap. The initial conditions for the channel temperature profile are a Gaussian radius of 10 mm and a maximum temperature of 14 kK.

is heated to the channel temperature, an amount of energy of $\mathrm{d}q_{elo}$ is required. This energy is given by

$$\mathrm{d}q_{elo} = \mathrm{d}V \int_{T_{amb}}^{T} \rho c_p \, \mathrm{d}T' \tag{17}$$

where $\rho$ is the mass density, $c_p$ is the heat capacitivity (heat capacity per unit mass) at isobaric transformations, $T = T(r)$ is the channel temperature and $T_{amb}$ is the temperature from which the air in $\mathrm{d}V$ must be heated. Thus, we have a local consumption rate of energy given by

$$Q_{elo} = \frac{\mathrm{d}q_{elo}}{\mathrm{d}t}. \tag{18}$$

For a cylindrical channel that is axially elongated with velocity $v_{elo}$, $\mathrm{d}V$ is given by

$$\mathrm{d}V = \mathrm{d}S \, \mathrm{d}l = 2\pi r \, \mathrm{d}r \, v_{elo} \, \mathrm{d}t \tag{19}$$

which gives

$$Q_{elo} = 2\pi v_{elo} r \, \mathrm{d}r \int_{T_{amb}}^{T} \rho c_p \, \mathrm{d}T'. \tag{20}$$

The influence of the elongation velocity for a current of 100 A is shown in figure 11. The figure shows the development over time of the linear resistance of the channel. The initial conditions for the channel temperature profiles are a Gaussian radius of 10 mm and a maximum temperature of 14 kK. These and further estimates of the influence of the channel elongation give the fact that the channel elongation velocity must be greater than 1000 m s$^{-1}$ to give any recognizable contribution. Thus, for the arc channel during a lightning swept stroke along an aircraft, the effect of channel elongation is negligible.

### 3.3. Thermal losses due to aerodynamic flow

The following model takes into account the thermal losses due to the increased convective cooling of the channel caused by a transverse airflow. The derivation of the model closely follows Bublievskii (1978). With the assumption of an impermeable channel core, the energy balance can be written as follows:

$$\rho c_p \frac{\mathrm{d}T}{\mathrm{d}t} = \sigma E^2 + \nabla(\kappa \nabla T). \tag{21}$$

At equilibrium, it reduces to

$$\sigma E^2 = -\frac{1}{r} \frac{\partial}{\partial r} \left( r \frac{\partial S}{\partial r} \right) \tag{22}$$

where $S = \int_0^T \kappa \, dT$ is the heat flux potential. Equation (22) can be integrated in a simple way if we assume constant electrical conductivity $\sigma$. This gives the following expression for the heat flux potential:

$$S = S^{00} - \sigma E^2 \frac{r^2}{4} \tag{23}$$

with $S^{00} = S(r = 0)$. Let $r^*$ be the radius where the heat flux by forced convection $q^*$ is equal to the conductive heat transfer. This equilibrium may be written as

$$q^* = \left| \frac{\partial S}{\partial r} \right|_{r=r^*}. \tag{24}$$

The heat flux $q^*$ by forced convection may be expressed as

$$q^* = h(T^* - T^\infty) \tag{25}$$

where $T^*$ is the temperature at radius $r^*$ and $T^\infty$ is the ambient temperature. $h$ is a coefficient that depends on the airflow characteristics at $r^*$; it can be expressed using the Nusseldt number $Nu$ which quantifies the heat transfer by forced convection and by conduction:

$$Nu = \frac{2hr^*}{\kappa^\infty}. \tag{26}$$

The Nusseldt number is related to the classical Reynolds number by $Nu = AR_e^m$. Furthermore, the Reynolds number associated to the airflow around an equivalent cylinder of radius $r^*$ is given by

$$R_e = \frac{r^* V^\infty \rho^\infty}{\mu^\infty} \tag{27}$$

where $V^\infty$ is the airflow velocity, $\rho^\infty$ is the air density and $\mu^\infty$ is the air viscosity. Thus, $q^*$ can be written, assuming $m = 1$, as

$$q^* = \frac{A\kappa^\infty V^\infty \rho^\infty (T^* - T^\infty)}{2\mu^\infty}. \tag{28}$$

The equilibrium of heat fluxes at $r^*$ then leads to the following equation, achieved by integrating (24):

$$S^* - S^{00} = \Delta S^{00} = -\frac{A\kappa^\infty V^\infty \rho^\infty (T^* - T^\infty)}{2\mu^\infty} r^*. \tag{29}$$

Using $I/\pi r^2 = \sigma E$, equation (23) can be written as

$$\Delta S^{00} = -\frac{\sigma E^2 r^{*2}}{4} = -\frac{I^2}{4\pi^2 r^{*2} \sigma}. \tag{30}$$

From equations (29) and (30), the radius $r^*$ and the internal electric field $E$ can be calculated where the input parameters are the current $I$, the temperature $T^*$ at the heat flux equilibrium surface and the average electrical conductivity $\sigma$. Bublievskii (1978) used the following parameters: $A = 0.2$, $\kappa^\infty = 2.7 \times 10^{-2}$ W m$^{-1}$ K$^{-1}$, $\rho^\infty = 1.18$ kg m$^{-3}$, $\mu^\infty = 1.86 \times 10^{-5}$ kg m$^{-1}$, $T^* = 7000$ K and $\sigma = 7.7 \times 10^3\ \Omega^{-1}$ m$^{-1}$, which result in a radius $r^*$ and an internal field $E$ given by:

$$r^* = 1.50 \times 10^{-4} \left( \frac{I^2}{V^\infty} \right)^{1/3} \tag{31}$$

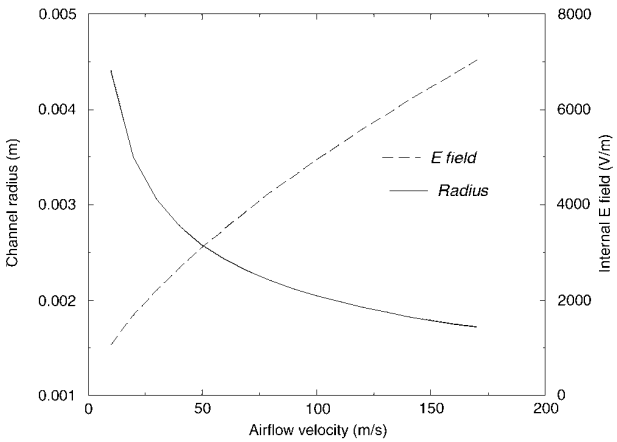


**Figure 12.** The internal electric field and the equivalent radius of an arc channel as a function of the speed of the transverse aerodynamic flow according to expressions (31) and (32) for a current of 500 A.

and

$$E = 1.83 \times 10^3 \left( \frac{V^{\infty 2}}{I} \right)^{1/3}. \tag{32}$$

These two quantities are illustrated for a current of 500 A in figure 12.

In the magnetically-swept stroke experiment (Dobbing and Hanson 1978) mentioned in section 2.2, the internal electric field of the arc was measured to be $E_{arc} = 2.4 \pm 0.48$ kV m$^{-1}$. The arc current was triangularly-shaped having a peak current of 3 kA, and the speed of the arc channel was 62 ms$^{-1}$. For this arc speed and with currents of 3 and 1.5 kA, (32) gives internal electric fields of 2.0 and 2.5 kV m$^{-1}$, respectively. The agreement between the experimental results and the calculated values is satisfying. The agreement with the rocket sled experiment is not satisfying, and this discussion is continued in the second part of this work (Larsson *et al* 2000) which contains modelling of the complete swept-stroke process. However, the Bublievskii model appears to give a consistent description of the arc channel as being a channel in equilibrium under the influence of a transverse aerodynamic flow, but the choice of values of the parameters in the model requires further experimental data to be thoroughly validated.

## 4. Conclusions

The main conclusions regarding the properties of the lightning channel during the continuous current phase of a lightning swept stroke are that the steady-state conditions are rapidly reached and that the channel can be considered to be a free-burning arc subjected to increased thermal losses due to a transverse aerodynamic flow. These observations are used in the second part of this work (Larsson *et al* 2000) which contains simulations of the complete swept-stroke process.

## Appendix. Molar mass of hot air

When air is heated, the nitrogen and oxygen molecules starts to dissociate into atomic nitrogen and oxygen, with nitric oxide as an intermediate product. This means that the molar

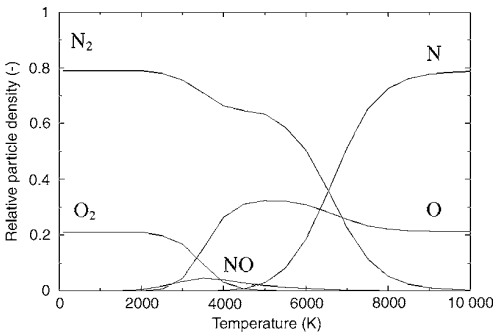


**Figure A1.** The relative densities of the different species in air as a function of the temperature.

mass of air is temperature dependent. In this appendix, the molar mass of air in equilibrium is calculated as a function of temperature. Furthermore, it is shown that equilibrium conditions are reached in a sub-millisecond time scale. The calculations are based on computer programs developed by Berton (1995).

### A.1. Molar mass of air at equilibrium

The equilibrium concentrations of $N_2$, $O_2$, N, O and NO are given by

$$\begin{cases} N_2 \Leftrightarrow 2N \\ O_2 \Leftrightarrow 2O \\ NO \Leftrightarrow N + O \end{cases} \tag{A1}$$

with the equilibrium coefficients

$$\begin{cases} K_1 = \dfrac{[N]^2}{[N_2]} \\ K_2 = \dfrac{[O]^2}{[O_2]} \\ K_3 = \dfrac{[N][O]}{[NO]}. \end{cases} \tag{A2}$$

The equilibrium coefficients $K_i$ are taken from Boldi (1992). Dalton's law stipulates that the sum of all partial pressures is equal to the total pressure. With the ideal gas law, this gives

$$([N_2] + [O_2] + [N] + [O] + [NO])RT = p \tag{A3}$$

where $T$ is the temperature, $p$ is the pressure and $R$ is the molar gas constant. The conservation of nitrogen and oxygen atoms can be expressed as

$$\frac{[N] + 2[N_2] + [NO]}{[O] + 2[O_2] + [NO]} = \frac{x_0}{y_0} \tag{A4}$$

where $x_0$ and $y_0$ are the relative abundances of nitrogen and oxygen atoms, respectively. For air, $x_0 = 0.79$ and $y_0 = 0.21$. Equations (A2)–(A4) give five equations for the five unknown concentrations. Figure A1 shows the relative particle densities for the different species as a function of temperature at atmospheric pressure. The dissociation starts at about 2 kK and is complete at about 10 kK.
If introducing

$$n = [N_2] + [O_2] + [N] + [O] + [NO]$$

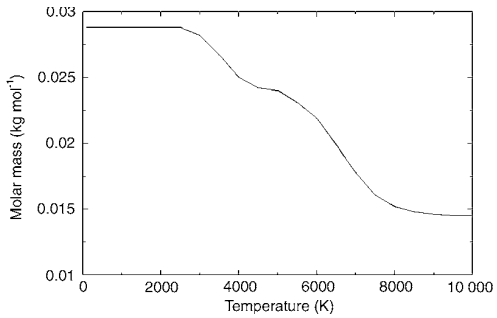


**Figure A2.** The molar mass of air as a function of the temperature.

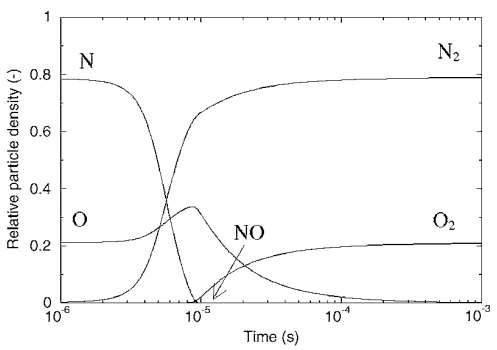


**Figure A3.** The evolution of air species when the air temperature is instantaneously decreased from 10 to 1 kK.

the molar mass $M$ of air can be expressed as

$$M = \frac{1}{n}(M_{N_2}[N_2]+M_{O_2}[O_2]+M_N[N]+M_O[O]+M_{NO}[NO])$$

with

$$M_{N_2} = 0.028 \text{ kg mol}^{-1}$$

$$M_{O_2} = 0.032 \text{ kg mol}^{-1}$$

$$M_N = 0.014 \text{ kg mol}^{-1}$$

$$M_O = 0.016 \text{ kg mol}^{-1}$$

$$M_{NO} = 0.030 \text{ kg mol}^{-1}.$$

In figure A2, the molar mass of air is presented as a function of the temperature. This curve is used in the arc column model.

### A.2. The decay of non-equilibrium

A change in the temperature will give rise to a deviation from the equilibrium concentrations, but after the temperature change the concentrations will relax to a new equilibrium. The response of air at equilibrium at 10 kK to a step decrease of the temperature to 1 kK is calculated. Figure A3 gives the evolution over time of the air species. However, the new equilibrium concentrations are reached within a fraction of a millisecond. This is sufficiently fast to allow the assumption of equilibrium concentrations of air species in lightning swept-stroke arc channels.

## References


Bacchiega G L, Gazzani A, Bernardi M, Gallimberti I and Bondiou A 1994 Theoretical modelling of the laboratory negative stepped-leader *Proc. 1994 Int. Aerospace and Ground Conf. on Lightning and Static Electricity, Mannheim, Germany*

Bailey J C and Anderson R V 1987 Experimental calibration of a vector electric field meter measurement system on an aircraft *NASA Research Report*

Berton R 1995 Evaluation theorique de la production de $NO_x$ dans la phase de refroidissement d'une decharge de foudre *ONERA Internal Report* No RT 11/6154 PN

Boldi R A 1992 A model of the ion chemistry of electrified convection *Doctoral Thesis* Massachusetts Institute of Technology

Bondiou A and Gallimberti I 1994 Theoretical modelling of the development of the positive spark in long gaps *J. Phys. D: Appl. Phys.* **27** 1252

Boulay J 1994 Interactions de la foudre sur un aéronef *ONERA Internal Report* No 5/6777 PN

Braginskii S I 1958 Theory of the development of a spark channel *Sov. Phys. JETP* **34** 1068

Bublievskii A F 1978 An approximate model of an electric arc in transverse mutually perpendicular aerodynamic and magnetic fields *J. Eng. Phys.* **35** 1424

Castellani A, Bondiou-Clergerie A, Lalande P, Bonamy A and Gallimberti I 1998a Laboratory study of the bi-leader process from an electrically floating conductor—part 1: general results *IEE Proc. Sci. Meas. Technol.* **145** 185

——1998b Laboratory study of the bi-leader process from an electrically floating conductor—part 2: bi-leader properties *IEE Proc. Sci. Meas. Technol.* **145** 193

Delalondre C and Simonin O 1990 Modelling of high intensity arcs including non-equilibrium description of the cathode sheath *J. Physique Coll.* **51** C5 199

Dobbing J A and Hanson A W 1978 A swept stroke experiment with a rocket sled *Int. Symp. on Electromagnetic Compatibility, Atlanta, GA*

Gallimberti I 1979 The mechanism of the long spark formation *J. Physique Coll.* **40** C7 193

Gallimberti I and Stangherlin S 1986 Thermodynamic decay of the leader channel after the discharge arrest *IEE Proc.* A **133** 431

Goelian N, Lalande P, Bondiou-Clergerie A, Bacchiega G L, Gazzani A and Gallimberti I 1997 Simplified model for the simulation of the positive spark development in long air gaps *J. Phys. D: Appl. Phys.* **30** 2441

Haidar J 1999 Non equilibrium modelling of transformed arcs *J. Phys. D: Appl. Phys.* **32** 263

Jones G R 1983 High current arcs at high pressures *16th Int. Conf. on Phenomena in Ionized Gases, Düsseldorf, Germany*

Lalande P 1996 Etudes des conditions de foudroiement d'une structure au sol *Thèse de doctorat* Université d'Orsay, Paris

Lalande P, Bondiou-Clergerie A and Laroche P 1999a Analysis of available in-flight measurements of lightning strikes to aircraft *Int. Conf. on Lightning and Static Electricity, Toulouse, France*

——1999b Computation of the initial discharge initiation zones on aircraft or helicopter *Int. Conf. on Lightning and Static Electricity, Toulouse, France*

Lalande P, Bondiou-Clergerie A, Laroche P, Eybert-Berard A, Berlandis J-P, Bador B, Bonarmy A, Uman M A, Rakov V A 1998 Leader properties by triggered lightning techniques *J. Geophys. Res.* **103** 14 109

Lalande P, Bondiou-Clergerie A, Laroche P, Ulmann A, Dimnet P, Bourrilelon J F, Tamin L, Douay A, Uhlig F and Gondot P 1999c Determination in laboratory of zone of initial lightning attachment on aircraft and helicopter *Int. Conf. on Lightning and Static Electricity, Toulouse, France*

Larsson A, Bondiou-Clergerie A and Gallimberti I 1998 Numerical modelling of inhibited electrical discharges in air *J. Phys. D: Appl. Phys.* **31** 1831

Larsson A, Lalande P and Bondiou-Clergerie A 2000 The lightning swept stroke along an aircraft in flight. Part II: numerical simulations of the complete process *J. Phys. D: Appl. Phys.* **33** 1876–83

Les Renardières Group 1977 Positive discharges in long air gaps at Les Renardières 1975 results and conclusions *Electra* **53** 86

Lowke J J, Voshall R E and Ludwig H C 1973 Decay of electrical conductance and temperature of arc plasmas *J. Appl. Phys.* **44** 3513

Maecker H 1971 Principles of arc motion and displacement *Proc. IEEE* **59** 439

Raizer Yu P 1997 *Gas Discharge Physics* (Berlin: Springer)

Uhlig F, Jones C, Vile M and Tagliana B 1999 Setup and statistical analysis of an database on in-flight lightning strike incidents *Int. Conf. on Lightning and Static Electricity, Toulouse, France*

Uman M A and Voshall R E 1968 Time interval between lightning strokes and the initiation of dart leaders *J. Geophys. Res.* **73** 497

Vérité J C, Boucher T, Comte A, Delalondre C, Robin-Jouan P, Serres E, Texier V, Barrault M, Chevrier P and Fievet C 1995 Arc modelling in $SF_6$ circuit breakers *IEE Proc. Sci. Meas. Technol.* **142** 189

von Engel A 1955 *Ionized Gases* (Oxford: Clarendon)

Zaglauer H, Wulbrand W, Douay A, Uhlig F, Jones C, Clibbon K, Ulmann A, Lalande P, Bondiou-Clergerie A and Laroche P 1999 Definition of lightning strike zones on aircraft and helicopters—results of the FULMEN program *Int. Conf. on Lightning and Static Electricity, Toulouse, France*